J|A|C|S ARTICLES

Published on Web 05/22/2009

The Temperature-Dependent Structure of Alkylamines and Their Corresponding Alkylammonium-Alkylcarbamates

Nataly Belman,[†] Jacob N. Israelachvili,[‡] Youli Li,[§] Cyrus R. Safinya,[⊥] Joel Bernstein,[¶] and Yuval Golan*,[†]

Department of Materials Engineering and Ilse Katz Institute of Nanotechnology, Ben-Gurion University of the Negev, Beer-Sheva 84105, Israel, Department of Chemical Engineering, and Materials Department, University of California, Santa Barbara, California 93106, Materials Research Laboratory, University of California, Santa Barbara, California 93106, Materials, Physics, and Molecular, Cellular, and Developmental Biology Departments, University of California at Santa Barbara, Santa Barbara, California 93106, and Department of Chemistry, Ben-Gurion University of the Negev, Beer-Sheva 84105, Israel

Received April 18, 2009; E-mail: ygolan@bgu.ac.il

Abstract: In spite of the wide use of alkylamine (AA) surfactants, little attention has been paid to their spontaneous reactivity in air. Exposure of AA surfactants to CO_2 results in the formation of alkylammonium-alkylcarbamate (AAAC) molecular pairs. The effect of hydrocarbon chain length on the reactivity of AAs was followed by monitoring mass gain vs time under atmospheric conditions as well as in a saturated CO_2 environment. The rates of conversion to AAAC decreased with hydrocarbon chain length. Indexed powder X-ray diffractograms and the corresponding unit cells are presented for all phases of AAs and AAACs with chain lengths of 14, 16, and 18 carbons. Temperature-resolved powder X-ray diffraction of AAACs indicated anisotropic thermal expansion occurring exclusively along the *a* direction of the unit cell.

Introduction

There is currently considerable interest in chemical systems and materials which can spontaneously capture ambient carbon dioxide (CO_2) and reversibly release it under mild conditions upon demand, allowing for removal of excessive CO_2 from the atmosphere, and at the same time, facilitating its exploitation for renewable energy applications such as photochemical reduction and artificial photosynthesis.[1−6] We have recently showed that alkylamine (AA) surfactants readily form alkylammonium-alkylcarbamate (AAAC) molecular pairs upon reaction with ambient CO_2 and that the extent of the AA-to-AAAC conversion can strongly affect nanoparticle synthesis.[7] Interestingly, despite the wide use of AA surfactants, their three-dimensional structure has not been reported, and no files exist for these materials in the JCPDS powder diffraction file database. In the present work, we outline the complex behavior of the different modifications of AAs and describe their temperature-dependent three-dimensional (3D) structure which has not been previously deciphered.

The reaction of alkylamines such as tetradecylamine (TDA, $C_{14}H_{29}NH_2$), hexadecylamine (HDA, $C_{16}H_{33}NH_2$), and octadecylamine (ODA, $C_{18}H_{37}NH_2$) with CO_2 to form the corresponding AAAC is reversible upon heating, according to reaction 1:[7−11]

$$2CH_3(CH_2)_nNH_2 + CO_2 \underset{\Delta}{\rightleftharpoons} NH_3^+(CH_2)_nCH_3 + CH_3(CH_2)_nNHCO_2^- \quad (1)$$

Hence, ODA can react with CO_2 under ambient conditions to give octadecylammonium octadecylcarbamate (OAOC), HDA to give hexadecylammonium hexadecylcarbamate (HAHC), and TDA to give tetradecylammonium tetradecylcarbamate (TATC). Therefore, unless stringent precautions are taken, pure AAs gradually change upon air exposure and convert into the corresponding AAACs. AA surfactant molecules are commonly used for surface passivation in nanoparticle synthesis.[12,13] The reaction kinetics of AAs with CO_2 appear to be crucial for the synthesis of AA-coated nanoparticles; controlled exposure of

[†] Department of Materials Engineering and Ilse Katz Institute of Nanotechnology, Ben-Gurion University of the Negev.
[‡] Department of Chemical Engineering, and Materials Department, University of California, Santa Barbara.
[§] Materials Research Laboratory, University of California, Santa Barbara.
[⊥] Materials, Physics, and Molecular, Cellular, and Developmental Biology Departments, University of California at Santa Barbara.
[¶] Department of Chemistry, Ben-Gurion University of the Negev.

(1) Barber, J. *Chem. Soc. Rev.* **2009**, *38*, 185–196.
(2) Benson, E. E.; Kubiak, C. P.; Sathrum, A. J.; Smeija, J. M. *Chem. Soc. Rev.* **2009**, *38*, 89–99.
(3) Benson, S. M.; Orr, F. M. *MRS Bull.* **2008**, *33*, 297–305.
(4) Gielen, D.; Newman, J.; Patel, M. K. *MRS Bull.* **2008**, *33*, 471–477.
(5) Gust, D.; Kramer, D.; Moore, A.; Moore, T. A.; Vermaas, W. *MRS Bull.* **2008**, *33*, 383–387.
(6) Hambourger, M.; Moore, G. F.; Kramer, D. M.; Gust, D.; Moore, A. L.; Moore, T. A. *Chem. Soc. Rev.* **2009**, *38*, 25–35.
(7) Belman, N.; Israelachvili, J. N.; Li, Y.; Safinya, C. R.; Bernstein, J.; Golan, Y. *Nano Lett.* **2009**, *9*, 2088–2093.
(8) George, M.; Weiss, R. G. *Langmuir* **2002**, *18*, 7124–7135.
(9) George, M.; Weiss, R. G. *Langmuir* **2003**, *19*, 1017–1025.
(10) George, M.; Weiss, R. G. *J. Am. Chem. Soc.* **2001**, *123*, 10393–10394.
(11) Holas, T.; Zbytovska, J.; Vavrova, K.; Berka, P.; Madlova, M.; Klimentova, J.; Hrabalek, A. *Thermochim. Acta* **2006**, *441*, 116–123.
(12) Acharya, S.; Patla, I.; Kost, J.; Efrima, S.; Golan, Y. *J. Am. Chem. Soc.* **2006**, *128*, 9294–9295.
(13) Belman, N.; Acharya, S.; Konovalov, O.; Vorobiev, A.; Israelachvili, J.; Efrima, S.; Golan, Y. *Nano Lett.* **2008**, *8*, 3858–3864.

AAs to CO_2 allowed reproducible formation of uniform, anisotropic ZnS nanoparticles with well-defined morphologies.[7]

Single crystal structure analysis performed by Bradley et al. on ODA indicated a herringbone molecular arrangement, with a space group $P2_1ab$. Axial lengths were $a = 5.60$ Å, $b = 7.35$ Å, and $c = 45.1$ Å. There were four molecules per cell, and each chain axis was inclined at 25.5° to the c-axis.[14] There are two important points to note about Bradley's work: (i) This limited conference abstract is the only report in the literature on the 3D structure of ODA; there has been no follow-up on Bradley's work, and no powder diffraction files exist for TDA, HDA, or ODA in the JCPDS database despite their wide use. (ii) There is no mention of their spontaneous reactivity in air. The crystal structures of TDA, HDA, and the three corresponding AAACs have never been published to date, and only their lamellar d-spacings were reported: $d_{TDA} = 35.38$ Å, $d_{HDA} = 40.51$ Å, $d_{TATC} = 42.0$ Å, $d_{HAHC} = 47.6$ Å, $d_{OAOC} = 52.4$ Å.[8,9]

The CO_2 reaction kinetics with very short-chain primary AAs (C_2−C_6) were previously studied by Singh et al.[15,16] The absorption rate and absorption capacity were shown to decrease with chain length of the absorbent molecule. Absorption of CO_2 has considerable environmental significance. CO_2 is a greenhouse gas and one of the major causes of global warming. Understanding of CO_2 absorption mechanisms and absorption kinetics, and development of methods for efficient recovery of absorption materials are likely to be crucial for technologies aimed at removal of greenhouse gases and their possible exploitation for renewable energy sources.[1−6,15−18] In the present work, the reaction kinetics of CO_2 with dodecylamine (DDA, $C_{12}H_{25}NH_2$), TDA, HDA, and ODA are compared both in saturated CO_2 environments and in atmospheric conditions. The 3D structural evolution of the AA-AAAC system is presented in detail using temperature-resolved powder X-ray diffraction (XRD), and the thermal expansion coefficients are derived.

Results and Discussion

AAAC Formation. The first stage of our work was to understand the chemical and structural changes occurring in AAs during exposure to air. Using an optical microscope equipped with a temperature-controlled stage, we monitored and recorded gas bubbles released during heating of TATC powder immersed in silicone oil. The bubbles were initially observed at ~60 °C and ceased upon sample melting at ~100 °C (heating rate was 4 °C/min). It was initially suspected that the reason for the bubbles was absorbed water. However, reactivity with water was ruled out using mass spectroscopy, Karl Fisher titration, and infrared spectroscopy.[7] Subsequently, first-year chemistry laboratory analysis was carried out to test for the presence of CO_2 in the bubbles evolving from aged (exposed to the ambient air) AA upon heating. The gas evolving from the heated AAs was collected and streamed into an aqueous calcium hydroxide solution. This positively identified the presence of CO_2 with the precipitation of $CaCO_3$ according to the reaction $Ca(OH)_2 + CO_2 \rightarrow CaCO_3 + H_2O$. The solid precipitate was indeed identified as calcium carbonate ($CaCO_3$) by energy dispersive spectrometry (EDS), which confirmed equal atomic amounts of Ca and C, and hence the gas evolving from AAs upon heating was unequivocally identified as CO_2. Reaction of CO_2 with two AA molecules results in the formation of one AAAC molecule pair, as illustrated in Figure 1. The exothermic reaction can be reversed by heating.[7−11]

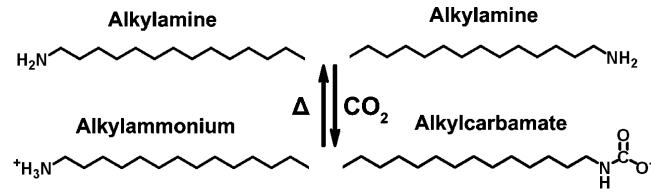

Figure 1. Schematic showing reversible AAAC formation by reaction of CO_2 with two AA molecules. The reaction is reversed by heating.

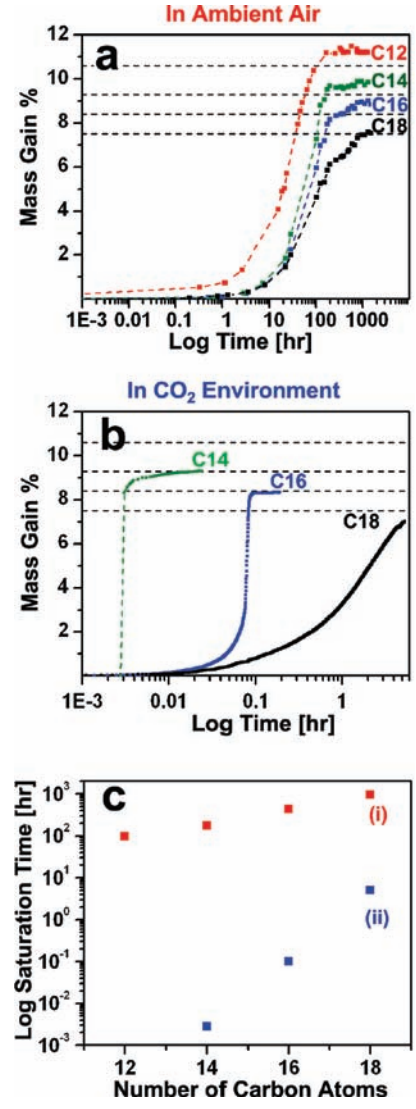

Figure 2. Mass gain percent as a function of air-exposure time for AAs with different chain lengths: DDA (C_{12}), TDA (C_{14}), HDA (C_{16}), and ODA (C_{18}). The dashed lines show the calculated values for the mass gain percent in saturated molecules. (a) Mass gain under atmospheric conditions. (b) Mass gain obtained in a TGA chamber saturated with CO_2. (c) Time required for CO_2 saturation vs AA chain length plotted for (i) atmospheric conditions (red), and (ii) saturated CO_2 environment (blue).

(14) Bradley, W. F.; Bellon, P. L.; Tassios, D. P. Am. Cryst. Assoc. (Winter Meeting), Tulane University, New Orleans, LA, March 2−3, 1970; The Structure of the Orthorhombic n-Alkylamines with Even-Numbered Carbon Chains. In *Abstracts of Papers*; Tulane University: New Orleans, LA; 1970; p 50.
(15) Singh, P.; Niederer, J. P. M.; Versteeg, G. F. *Int. J. Greenhouse Gas Control* **2007**, *1*, 5–10.
(16) Singh, P.; Versteeg, G. F. *Process. Saf. Environ. Prot.* **2008**, *86*, 347–359.
(17) Belić, D. S. *Facta Universitatis - Series: Physics, Chemistry and Technology* **2006**, *4* (1), 45–55.
(18) Zamostny, P.; Kukula, P.; Young, J. S. *Chem. Listy* **1999**, *93*, 238–242.

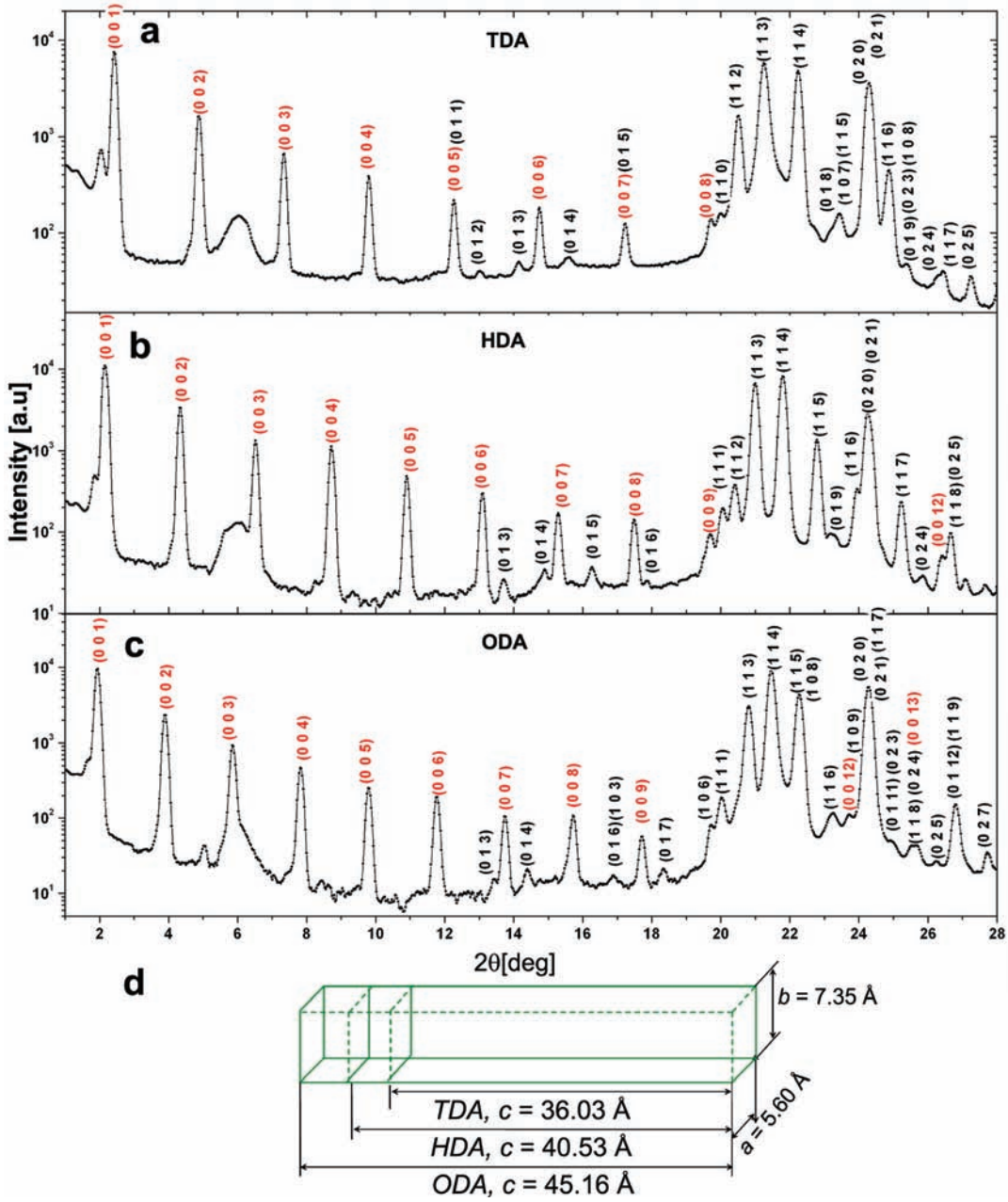

Figure 3. Powder XRD patterns and Bragg peak indexing of pure AAs at room temperature. The fundamental (*0 0 1*) lamellar peak and its high-order reflections (*0 0 l*) are marked in red. (a) TDA, (b) HDA, and (c) ODA. (d) Schematic representation of the corresponding AA unit cells.

CO_2 Absorption Kinetics. Mass gain gravimetry experiments were carried out in order to assess the absorption rate and total CO_2 absorption capacities of ODA, HDA, TDA, and DDA. For mass gain experiments, the AAs were purified to be free of CO_2 by melting prior to the measurements to release remnant CO_2, cooled down under argon and ground. Mass gain percent as a function of air-exposure time in AAs with different chain lengths is plotted in Figure 2a: DDA with 12 carbon atoms in the hydrocarbon chain, TDA with 14, HDA with 16 and ODA with 18 carbon atoms. We find that AAs of different chain lengths do not adsorb CO_2 at the same rate. The dashed lines show the calculated values for the mass gain percent at CO_2 saturation (at a 2:1 AA/CO_2 ratio according to reaction 1): 10.6, 9.3, 8.4, and 7.5%, respectively. The logarithmic time dependence of CO_2 saturation in AAs and complete formation of the corresponding AAACs on hydrocarbon chain length in atmospheric conditions is shown in Figure 2c (plot i, red points): 95 h for DDA, 174 h for TDA, 430 h for HDA, and 940 h for ODA. In a separate experiment, AA powder samples were placed in a TGA chamber saturated with CO_2. The shorter-chain molecules (DDA) reacted very rapidly and reached saturation within seconds (not shown, since the reaction was too fast to monitor). TDA was saturated in ~15 s, HDA in 6 min and ODA in 5 h, as shown in Figure 2b. The resulting time for saturation in a CO_2-rich environment is plotted in Figure 2c (plot ii, blue points). In both experiments, the reaction rate of AAs with CO_2 clearly decreased with hydrocarbon chain length (longer time required for CO_2 saturation). Note that increasing chain length increases the molecular weight; therefore, the CO_2 mass percent in the AAs is expected to decrease with hydrocarbon chain length. These results are in agreement with previous studies by Singh et al.[15,16] who showed that increasing chain length resulted

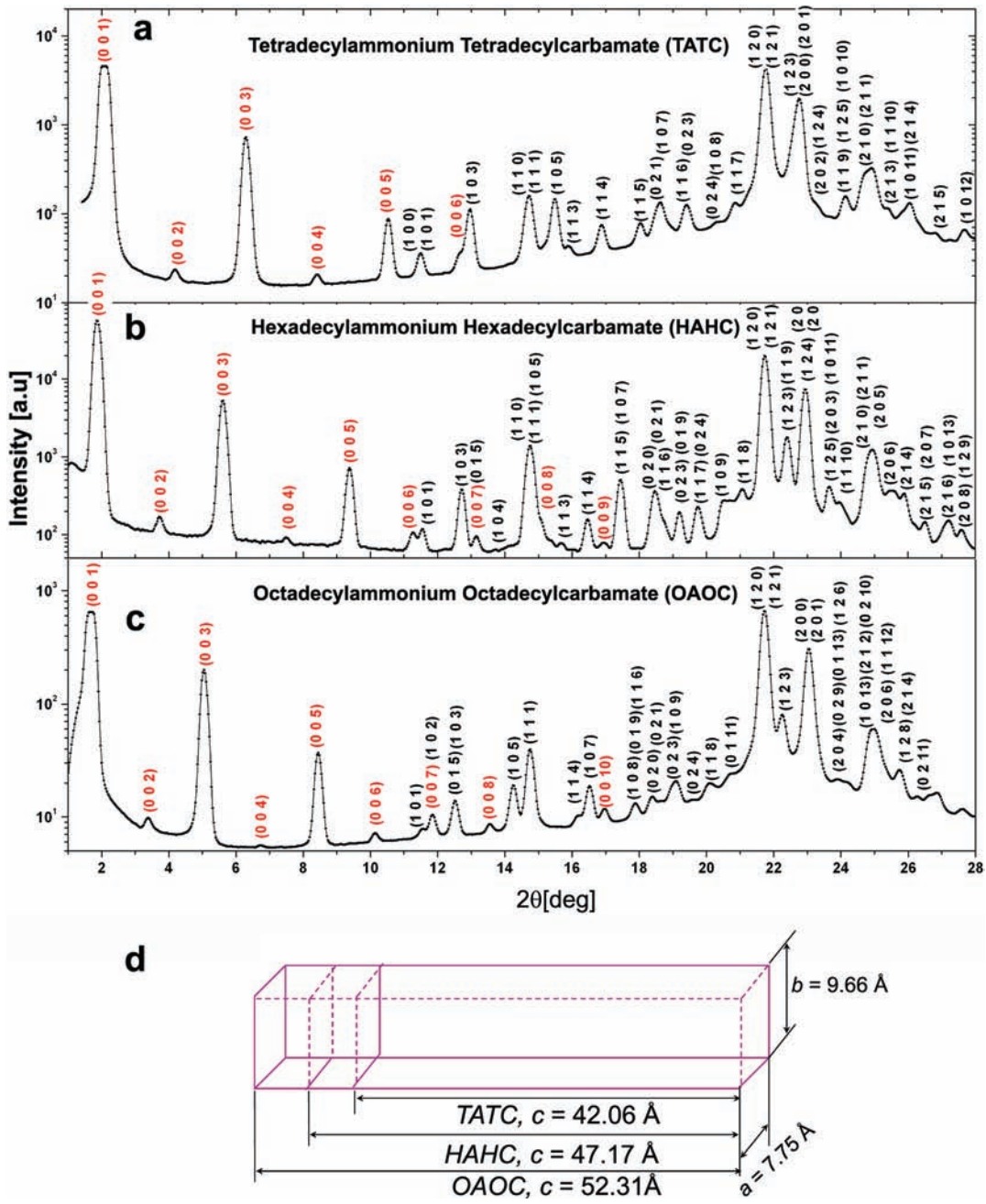

Figure 4. Powder XRD patterns and Bragg peak indexing of the fully converted AAACs at room temperature: (a) TATC, (b) HAHC, and (c) OAOC. (d) Schematic representation of the corresponding AAAC unit cells.

in decreased CO_2 absorption rate and absorption capacity for short-chain primary AAs (C_2-C_6).

Table 1. Phase Transition Temperature [°C] upon Heating of the AAs and their AAACs Obtained from DSC Measurements[a]

	Phase Transition Temperature [°C]		
	1st cycle		2nd cycle
TDA, $C_{14}H_{29}NH_2$	41.3		40.3
HDA, $C_{16}H_{33}NH_2$	49.9		49.5
ODA, $C_{18}H_{37}NH_2$	55.0		54.2
TATC, $C_{14}H_{29}NHCO_2^- + C_{14}H_{29}NH_3^+$	83.6	98.1	39.2
HAHC, $C_{16}H_{33}NHCO_2^- + C_{16}H_{33}NH_3^+$	93.3	99.8	47.6
OAOC, $C_{18}H_{37}NHCO_2^- + C_{18}H_{37}NH_3^+$	96.6	101.9	53.9

[a] Note that the AAACs showed two transitions upon heating, pointing out the presence of a so-called "high-temperature AAAC structure" prior to melting. The temperature measurement error was ±0.5 °C.

Powder XRD Investigation. Powder X-ray diffractograms obtained for TDA, HDA, and ODA at room temperature are shown in Figure 3. The presence of a large number of Bragg peaks in the spectrum is indicative of a highly ordered surfactant assembly. The lamellar packing of the molecules is evident from a set of high-order peaks corresponding to the lamellar spacing, with up to 12 orders of diffraction observed in the diffractogram. The peaks were indexed to an orthorhombic unit cell with the same in-plane lattice constants $a = 5.60$ Å, $b = 7.35$ Å for all three chain lengths, while the lamellar spacing scaled, as expected, with chain length: $c = 36.03$, 40.53, and 45.16 Å for TDA, HDA, and ODA, respectively.[7] The error in the calculated lattice constants is ±0.04 Å. The (h k l) Miller indices are noted above each peak.

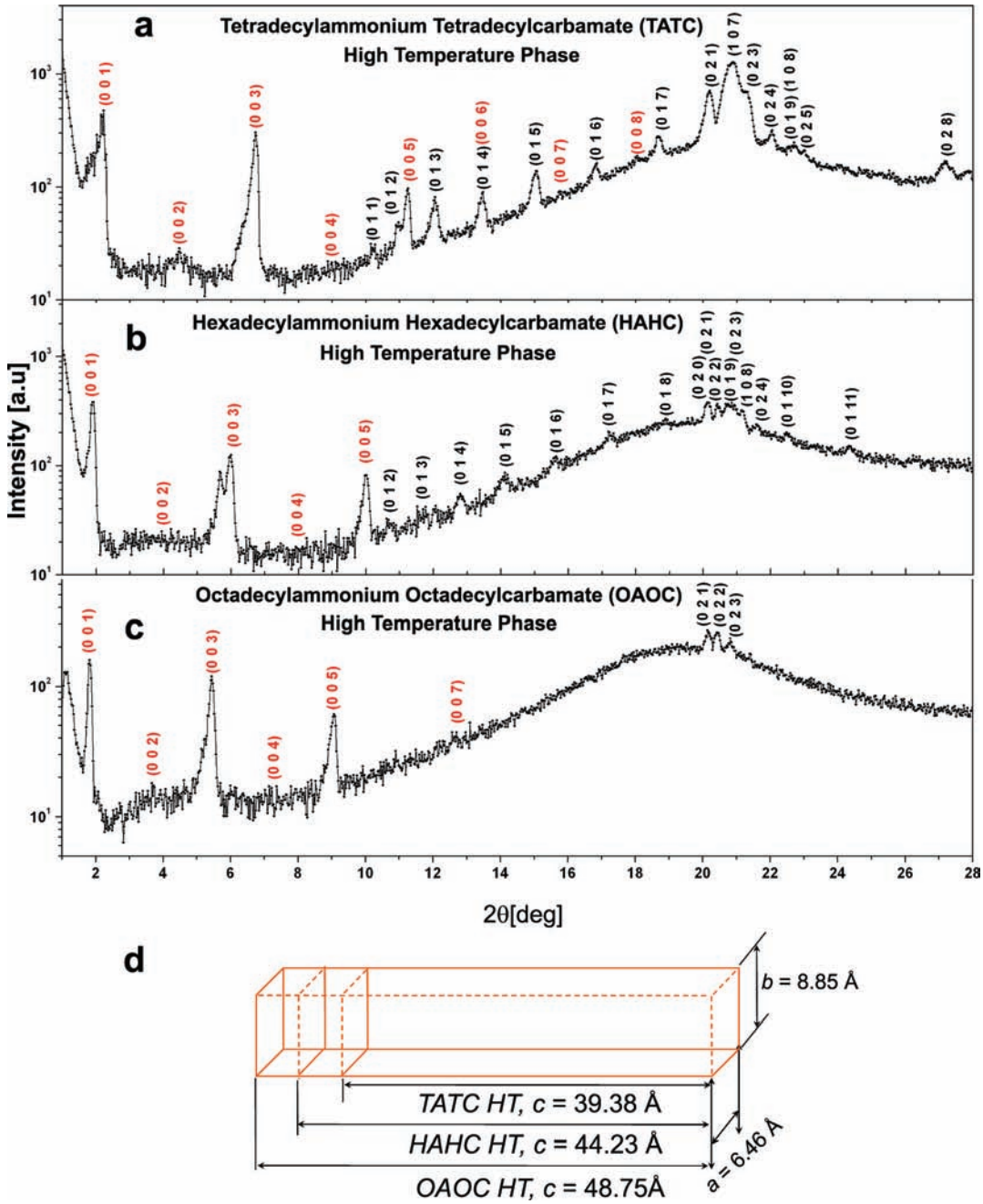

Figure 5. Powder XRD patterns and corresponding indexing of the metastable high-temperature structures of (a) TATC at 79 °C, (b) HAHC at 89 °C, and (c) OAOC at 92 °C. (d) Schematic representation of the unit cells of the three high-temperature structures of AAACs.

Exposure of the AAs to CO_2 was carried out by placing the pure AA sample in a desiccator with dry ice until weight gain reached saturation. The fully converted AAAC samples had an orthorhombic unit cell where all three lattice constants were now *different* (Figure 4): the in-plane lattice constants were the same for the three chain lengths $a = 7.75$ Å, $b = 9.66$ Å, while the lamellar spacing scaled with chain length: $c = 42.06$, 47.17, and 52.31 Å for TDA, HDA, and ODA, respectively.

Differential scanning calorimetry (DSC) identified solid-state phase transitions and provided the melting points of the surfactants.[7] Upon heating AAAC powders from 10 to 150 °C at a heating rate of 5 °C/min, endothermic peaks were observed

Table 2. Unit Cell Dimensions for the Pure Alkylamines (TDA, HDA, ODA; Figure 3), and for the Room Temperature (Figure 4) and High Temperature Phases of Alkylammonium-Alkylcarbamates (TATC, HAHC, OAOC) Derived from Temperature-Resolved Powder XRD Measurements (Figure 5)

	alkylamine (AA)			alkylammonium-alkylcarbamate (AAAC) room temperature (RT)			AAAC high temperature (HT)		
	a [Å]	*b* [Å]	*c* [Å]	*a* [Å]	*b* [Å]	*c* [Å]	*a* [Å]	*b* [Å]	*c* [Å]
C14	5.60	7.35	36.03	7.75	9.66	42.06	6.46	8.85	39.38
C16	5.60	7.35	40.53	7.75	9.66	47.17	6.46	8.85	44.23
C18	5.60	7.35	45.16	7.75	9.66	52.31	6.46	8.85	48.75

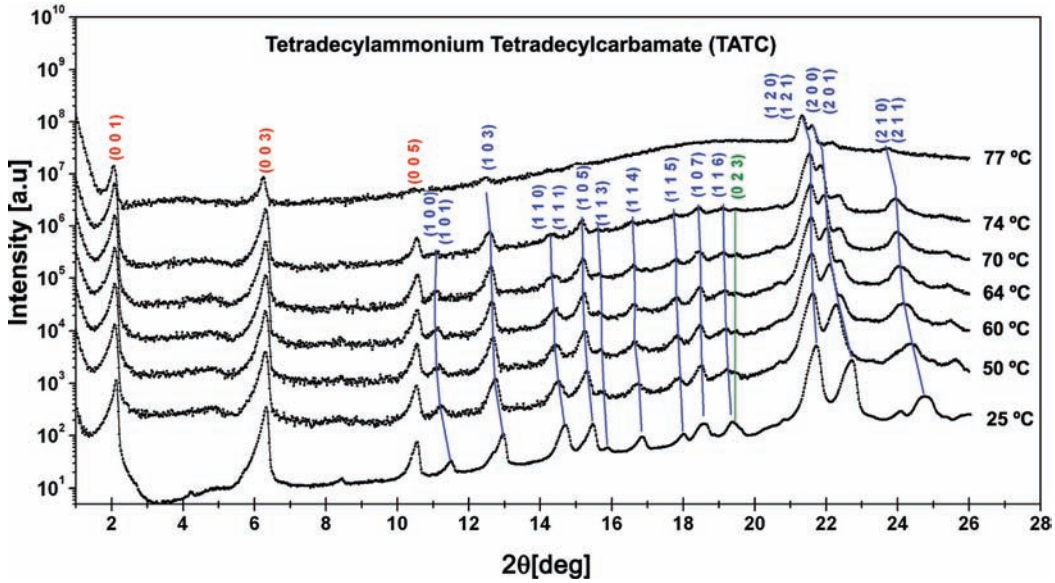

Figure 6. Temperature-resolved powder XRD patterns of TATC. Starting at room temperature (25 °C), TATC powder was heated to 50, 60, 64, 70, 74, and 77 °C (heating rate: 1 °C/min). The blue lines denote peaks shifting with temperature. Corresponding data for HAHC and OAOC is provided in Figure S1 (SI).

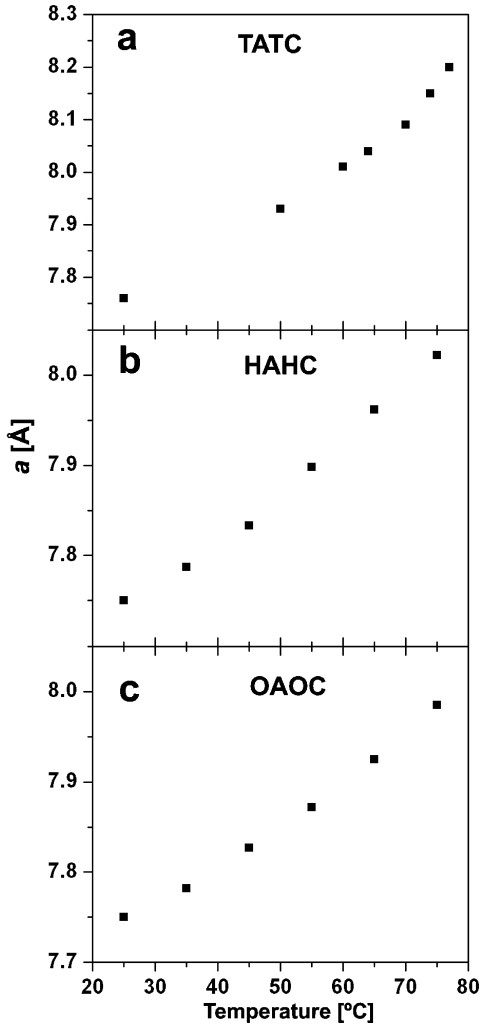

Figure 7. Temperature dependence of the lattice parameter *a* for (a) TATC, (b) HAHC, and (c) OAOC, respectively.

in the thermograms prior to melting (Table 1), indicating a solid-state structural transition. Correspondingly, a new metastable high temperature (HT) structure was identified also by XRD upon rapid heating of TATC to 79 °C, HAHC to 89 °C, and OAOC to 92 °C at a rate of 10 °C/min. This structure was indexed as an orthorhombic unit cell with the same in-plane lattice constants $a = 6.46$ Å, $b = 8.85$ Å for all three chain lengths (Figure 5). The lamellar spacing of the metastable HT structure was $c = 39.38$, 44.23, and 47.75 Å for TATC, HAHC and OAOC, respectively. The lattice constants of the AA unit cells are summarized in Table 2 and the complete list of indexed (*h k l*) reflections with corresponding *d*-spacings are detailed in Tables S1−S3 in the Supporting Information for the AAs and two phases of AAACs.

DSC thermograms of the second heating cycle of AAACs (after first cycle of heating to 150 °C and cooling down to 10 °C) showed phase transitions at melting points very close to those of pure AA (Table 1), indicating a reversible phase transition upon release of CO_2.

Temperature-Dependent Structural Evolution of AAACs. The structural changes observed in AAACs upon gradual heating are shown in Figure 6 for TATC and in Figure S1, Supporting Information (SI) for HAHC and OAOC. The temperature-resolved XRD patterns were recorded in the range 25 − 77 °C at a heating rate of 1 °C/min. Although there were no dramatic changes in the XRD patterns in the above-mentioned temperature range, part of the Bragg peaks clearly shifted toward lower angles with temperature, indicating directional expansion of the lattice. The blue lines in Figures 6 and S1 point at peaks which shifted with temperature. It can be clearly seen that the lamellar distance *c* remained constant with temperature, since peaks of the type (*0 0 l*) did not shift upon heating. The lattice constant change was calculated using the orthorhombic structure equation:

$$1/d^2 = h^2/a^2 + k^2/b^2 + l^2/c^2 \qquad (2)$$

The *a* lattice parameter was calculated using Equation 2 by substituting the experimentally obtained *d*-spacings for (*h k l*) reflections independent of the *b* lattice parameter (of the type

Table 3. Measured *a* Lattice Parameters and Thermal Expansion Coefficients α_a for All Three AAACs

TATC			HAHC			OAOC		
$C_{14}H_{29}NHCO_2^- + C_{14}H_{29}NH_3^+$			$C_{16}H_{33}NHCO_2^- + C_{16}H_{33}NH_3^+$			$C_{18}H_{37}NHCO_2^- + C_{18}H_{37}NH_3^+$		
T [K]	*a* [Å]	$\alpha_a[10^{-4}/\ °C]$	*T* [K]	*a* [Å]	$\alpha_a[10^{-4}/\ °C]$	*T* [K]	*a* [Å]	$\alpha_a[10^{-4}/\ °C]$
25	7.763	–	25	7.750	–	25	7.750	–
50	7.934	8.80	35	7.787	5.73	35	7.782	5.45
60	8.007	8.99	45	7.833	5.86	45	7.827	5.63
64	8.043	9.25	55	7.898	6.72	55	7.872	5.67
70	8.092	9.44	65	7.962	7.11	65	7.925	5.98
74	8.153	10.20	75	8.022	7.23	75	7.985	6.32
77	8.199	10.80						

(*h 0 l*)). The lattice parameter $c = 42.06$, 47.17, and 52.31 Å, respectively, for TATC, HAHC and OAOC was easily obtained from the lamellar peaks of the type (*0 0 l*). The variation of the average lattice parameter *a* with temperature is plotted in Figures 7a−c and summarized in Table 3.

Subsequently, it was established that the *b* lattice parameter was not affected by temperature. The first evidence was that the (*0 2 3*) and (*0 1 5*) reflections did not shift with temperature (marked with green lines in Figures 6 and S1a (SI)). The second evidence was obtained by calculating the *a* lattice parameter from reflections other than of the type *(h 0 l*). When the *a* lattice parameter was calculated using a constant lattice parameter $b = 9.66$ Å for all three AAACs and a constant parameter $c =$ 42.06, 47.17, and 52.31 Å for TATC, HAHC and OAOC, respectively (see Figure 5d), the change in lattice parameter *a* with temperature was the same. Therefore, we conclude that the thermal expansion of AAACs occurs exclusively along the *a* direction of the orthorhombic structure.

The calculated lengths of AAAC pairs (44.9, 49.9, and 54.9 Å for TATC, HAHC and TATC, respectively) in their extended conformations are ∼2.7 Å longer than the lamellar spacings measured from XRD. Hence, it is reasonable to assume that the AAAC molecules are tilted from the *c*-axis by ∼20°. This calculated angle is reasonably close to that previously suggested by George et al. for OAOC (18°).[9] Since thermal expansion apparently takes place only along the *a* axis, it is likely that the molecules are tilted from the *c*-axis toward the *a*-axis. Precise information on the atomic positions in these structures will require a full structure determination, yet our attempts have shown that growth of crystals with suitable size for single crystal XRD is tricky and complicated both for AAs and AAACs.

The measured lattice parameter *a* values were used for calculating the temperature dependent thermal expansion coefficients (α_a), defined as:[19]

$$\alpha_a = (1/a_{25})[(a_T - a_{25})/(T - 25)] \quad (3)$$

where a_T represents the lattice parameter *a* at temperature *T* and a_{25} is the corresponding value at 25 °C. The calculated values of thermal expansion coefficient α_a are listed in Table 3 over the entire temperature range observed.

The thermal expansion of AAs was not measured due to their rapid reaction with CO_2 and subsequent AAAC formation, which would strongly affect Bragg peak shifting in addition to the effect of thermal expansion.

In summary, the reaction rates of CO_2 with AAs decreased with hydrocarbon chain length and so did their total absorption capacity. Detailed powder XRD characterization and complete peak indexing provided the unit cell structures of all three different AAs and of the RT and HT phases of all three different AAACs. The temperature dependence of the AAAC structures was investigated, showing anisotropic thermal expansion of AAAC that exclusively occurs along the *a* direction of the orthorhombic unit cell, while lattice parameters *b* and *c* remained constant.

Acknowledgment. We thank D. Mogilyanski and I. Feldman for facilitating XRD measurements, A. Miliontshick for assistance with TGA, and A. Waserblat for the EDS/SEM measurements. This work was supported by the US-Israel Binational Science Foundation, Grant #2006032. This work made use of MRL Central Facilities supported by the MRSEC Program of the National Science Foundation under award No. DMR05-20415. Dedicated in memory of Prof. Shlomo Efrima.

Supporting Information Available: Detailed description of materials and methods. Tables of powder X-ray diffraction data, including diffraction angles, Miller indices and corresponding *d*-spacings for the diffractograms shown in Figures 3−5. Temperature-resolved powder XRD patterns of HAHC and OAOC. This material is available free of charge via the Internet at http://pubs.acs.org.

JA902944T

(19) Qin, P.; Chen, Y.; Liu, H.; Nong, L.; Zeng, L. *J. Alloys Compd.* **2008**, *463*, 34–37.